The Astrophysical Journal, 691:531–536, 2009 January 20 doi:10.1088/0004-637X/691/1/531

GAUGING THE DARK MATTER FRACTION IN AN L_* S0 GALAXY AT $z = 0.47$ THROUGH GRAVITATIONAL LENSING FROM DEEP *HUBBLE SPACE TELESCOPE*/ADVANCED CAMERA FOR SURVEYS IMAGING*

G. Covone[1,2,3], M. Paolillo[1,3], N. R. Napolitano[2], M. Capaccioli[1,4], G. Longo[1], J.-P. Kneib[5], E. Jullo[5,6], J. Richard[7], O. Khovanskaya[8], M. Sazhin[8], N. A. Grogin[9], and E. Schreier[10]
[1] Dipartmento di Scienze Fisiche, Università di Napoli "Federico II," Naples, Italy; covone@na.infn.it
[2] INAF–Osservatorio Astronomico di Capodimonte, Naples, Italy
[3] INFN, Naples, Italy
[4] INAF–VSTCeN, Naples, Italy
[5] LAM-CNRS, OAMP, Marseille, France
[6] ESO, Santiago, Chile
[7] Department of Astrophysics, California Institute of Technology, Pasadena, USA
[8] Sternberg Astronomical Institute, Moscow State University, Moscow, Russia
[9] School of Earth and Space Exploration, Arizona State University, Tempe, AZ 85287, USA
[10] Associated Universities Inc., Washington, DC 20036, USA
Received 2007 August 28; accepted 2008 September 24; published 2009 January 15

ABSTRACT

We analyze a new gravitational lens OAC–GL J1223–1239, serendipitously found in a deep I_{814}-band image of the *Hubble Space Telescope* (*HST*) Advanced Camera for Surveys (ACS). The lens is an L^*, edge-on S0 galaxy at $z_l = 0.4656$. The gravitational arc has a radius of $0\farcs42 \simeq 1.74\,h^{-1}$ kpc. We have determined the total mass and the dark matter (DM) fraction within the Einstein radius R_E as a function of the lensed source redshift, which is presently unknown. For $z_s \sim 1.3$, which is in the middle of the redshift range plausible for the source according to some external constraints, we find the central velocity dispersion to be $\sim 180\,\mathrm{km\,s^{-1}}$. With this value, close to that obtained by means of the Faber–Jackson relation at the lens redshift, we compute a 30% DM fraction within R_E (given the uncertainty in the source redshift, the allowed range for the DM fraction is 25%–35% in our lensing model). When compared with the galaxies in the local universe, the lensing galaxy OAC–GL J1223–1239 seems to fall in the transition regime between massive, DM-dominated galaxies and lower-mass, DM-deficient systems.

Key words: dark matter – galaxies: bulges – galaxies: structure – gravitational lensing

Online-only material: color figures

1. INTRODUCTION

Strong gravitational lensing (GL) is a valuable astrophysical tool to investigate the structure and evolution of early-type galaxies up to a redshift of ~ 1 (e.g., Keeton et al. 1998; Rusin et al. 2003; Treu et al. 2005) and to gauge the dark mater (DM) content at various galaxian scales (e.g., Treu et al. 2006; Jiang & Kochanek 2007). This tool offers the advantage of constraining the total mass within the Einstein radius independently of the dynamical status of the lensing galaxy. The technique is challenging to apply to low-luminosity lenses (LLLs); however, as the GL cross section is proportional to the fourth power of the central velocity dispersion (e.g., Covone et al. 2005). This is why LLLs appear far more rare than more massive systems. Their systematically smaller Einstein radii make strong lensing arcs around them hard to find with optical surveys. For instance, a lensing galaxy with velocity dispersion $\sigma_L \sim 200\,\mathrm{km\,s^{-1}}$ at $z_l \sim 0.5$, coupled to a source at $z_S \sim 1.0$, produces an Einstein ring with radius $\theta_E \sim 0\farcs5$. As a comparison, in a visual search for gravitational lenses in the COSMOS survey[11] (Faure et al. 2008), no lensing galaxy was found with central velocity dispersion smaller than $200\,\mathrm{km\,s^{-1}}$, out of a sample of 20 secure systems.

Although difficult to discover, LLLs are of great interest regarding recent claims of DM-deficient L_* galaxies in the local universe (see e.g., Capaccioli et al. 2003; Romanowsky et al. 2003; Napolitano et al. 2005 (N+05 hereafter); Douglas et al. 2007; Napolitano et al. 2009). Furthermore, these systems occupy a region of the luminosity/mass distribution in between boxy/slow-rotator systems and disky/fast-rotator systems (Nieto & Bender 1989; Capaccioli et al. 1992). The dichotomy of these systems appears to involve also their DM properties, either at effective radii scales (Cappellari et al. 2006) or beyond (Capaccioli et al. 2003, N+05).

This paper analyses an L_* edge-on S0 lensing galaxy at $z_l = 0.4656 \pm 0.0004$, hereafter named OAC–GL J1223–1239, serendipitously discovered in the *Hubble Space Telescope* (*HST*)/Advanced Camera for Surveys (ACS) follow-up imaging of a former candidate lensing cosmic string (Sazhin et al. 2007). The mean radius of the gravitational arc is $\theta_E = 0\farcs42$, corresponding to a linear radius of $1.74\,h^{-1}$ kpc, slightly larger than the estimated value of the effective (half-light) radius $R_{\rm eff}$ of the lens bulge (i.e., $\theta_E \sim 1.15\,R_{\rm eff}$). This compact arc offers the rare opportunity to gauge the mass distribution within the effective radius of an L_* galaxy at $z \sim 0.5$. Note that, among the 20 strong GLs found in the 1.64 square degrees of the COSMOS survey by Faure et al. (2008), selected in the range $0.2 < z < 1.0$ and median redshift 0.71, only one lens exhibits an arc with an angular radius smaller than $0\farcs40$.

As the redshift of the lensed source is yet unknown, despite two spectroscopic runs (see Section 2), the DM content of the lens cannot be unambiguously determined. However, by requiring that the lensing galaxy follows the Faber–Jackson relation (Faber & Jackson 1976), and exploiting the decoupled

* Based on observations made with ESO Telescopes at the La Silla Observatories and the NASA/ESA Hubble Space Telescope.
[11] http://cosmosstronglensing.uni-hd.de/

Table 1
Broad-Band Photometry of the Lens OAC–GL J1223-1239

Band	Total Mag
WFI B	22.74 ± 0.05
WFI V	21.86 ± 0.04
WFI R	20.85 ± 0.03
ACS F775	20.01 ± 0.06
ACS F814	20.04 ± 0.05

Table 2
Photometric Properties of the Lensing Galaxy, as Observed in the Band I_{814}

	mag	q	P.A. (deg)	$R_{\rm eff}$	$R_{\rm eff}$ (kpc)
bulge	20.45	0.35	−13.6	0.″37	1.54
disk	21.59	0.25	−8.4	0.″77	3.16

Note. q is the ratio of the two galaxy axes.

geometry of the luminosity and the total mass, we can then constrain the DM fraction within the Einstein radius R_E. Toward this end, in Section 3 we present a lensing model, and in Section 4 we infer the luminous mass from the analysis of the spectrophotometric data, in order to disentangle the lensing contribution of the DM from that of the total mass. In Section 5, we discuss the best mix of dark and luminous mass which produces the measured total mass as a function of the (unknown) source redshift, and draw conclusions in Section 6.

Throughout the paper we will assume a cosmological model with $\Omega_{\rm m} = 0.27$, $\Omega_\Lambda = 0.73$, and $h \equiv H_0/(100\,{\rm km\,s^{-1}\ Mpc^{-1}}) = 0.7$. At the lens redshift, 1″ corresponds to $4.15\,h^{-1}$ kpc (Komatsu et al. 2008). Magnitudes are in the AB system.

2. THE DATA

The gravitational lens OAC–GL J1223–239 (R.A.$_{\rm J2000}$ = $12^{\rm h}23^{\rm m}32\overset{\rm s}{.}65$; dec.$_{\rm J2000}$ = $-12^\circ39'40\overset{''}{.}7$) falls in the Osservatorio Astronomico di Capodimonte Deep Field (OACDF, Alcalá et al. 2004), a survey performed with the 2.2 m Wide Field Imager (WFI) in three broad bands (B, V, R) and six intermediate filters over the wavelength range 7730–9130 Å. OACDF broadband photometry and coordinates of the lens are given in Table 1. The spatial resolution (FWHM ∼ 1″) of the best-stacked OACDF image (R band, limiting magnitude $R = 25.1$) was not sufficient to resolve the gravitational arc, which was instead discovered serendipitously by *HST* observations.

The latter are deep *HST*/ACS WFC follow-up images[12] collected through the F814W filter (I_{814} in the following) for a total exposure time of 15 ks. A 1/3 pixel dither pattern (0.″05 per pixel) was adopted for subpixel sampling of the *HST* PSF and for cosmic ray rejection. The stacked image, obtained by combining the 12 exposures through the software Multidrizzle (Koekemoer et al. 2002), has 0.″025 per pixel sampling with spatial resolution of 0.″10 and 5σ detection limit of ∼ 27.3 mag arcsec^{-2} (see details in Sazhin et al. 2007). The *HST*/ACS image of the lensing system is shown in the left panel of Figure 1. In the right panel of Figure 1, we show the residuals after subtracting the lens photometric model in order to enhance

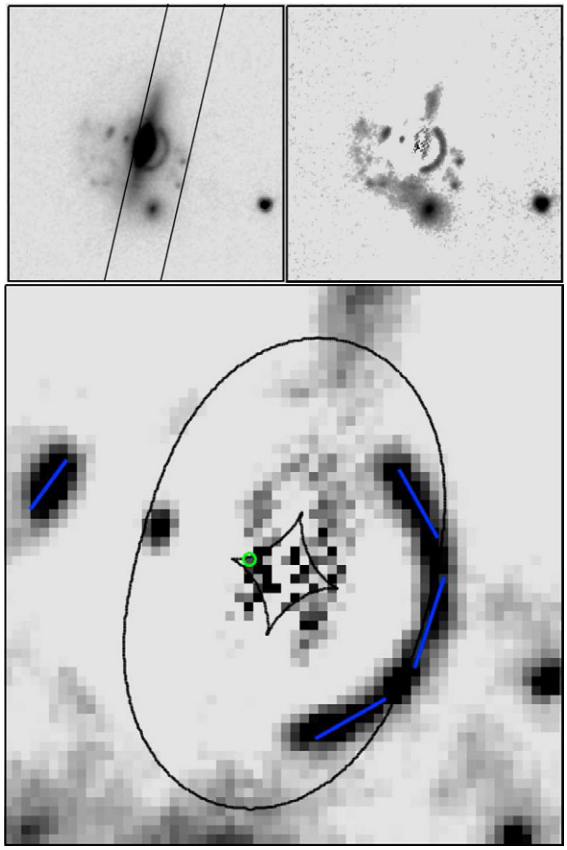

Figure 1. Left panel: *HST*/ACS image of the lensing system in the I_{814} filter; the position of the slit used in the Keck/LRIS spectroscopic observations is shown; field size is 5″ × 5″. Right panel: same sky region, after subtracting the photometric model of the lensing galaxy. Lower panel: the arc and counter-image positions (blue), caustics and critical line (black), predicted source location and size (green). Field size is 1.″5 × 1.″5.

(A color version of this figure is available in the online journal.)

the details of the lensed images. The model is based on the surface photometry performed with the tool `galfit` (Peng et al. 2002). The best-fit model requires two photometric components: an $r^{1/4}$ (de Vaucouleurs 1948) bulge combined with an exponential disk. The photometric parameters are given in Table 2. Both the photometric model and the spectroscopic data (discussed below) confirm that the lensing galaxy is an edge-on S0.

The gravitational arc, subtending ∼ 150°, is located at 0.″42 from the lens center, perpendicular to the minor axis of the galaxy. A candidate counter image appears on the opposite side at 0.″65. The nature of the other sources around the galaxy is unclear: they could be part of the S0 galaxy and/or could be background objects, possibly linked with the strongly lensed source.

The spectroscopic information of the OAC–GL J1223–1239 rests on data collected in two distinct observing runs. A low-resolution spectrum was obtained in 2000 April with the ESO Multi-Mode Instrument at the New Technology Telescope (NTT) in the multiobject spectroscopy mode, within a survey of color-selected early-type galaxies at intermediate redshift. Recently (while the paper was under revision), a long-slit medium resolution spectrum has been secured with the Low Resolution Imaging Spectrometer (LRIS) at the Keck I Telescope.

The total exposure time of the NTT spectrum was 3 × 2400 s, with a slit of 1 arcsec and the grism No. 3, yielding a dispersion

[12] Proposal ID 10715, PI: M. Capaccioli. The same field was also observed with *HST*/ACS by the program 10486, using filters F775W and F606W and with shorter exposures (2409 s and 5062 s, respectively). However, the filter F775W covers very similar wavelength range to the I_{814} image, offering no additional information, and in the F606W-band data our target is a few arcsec out of the field of view.

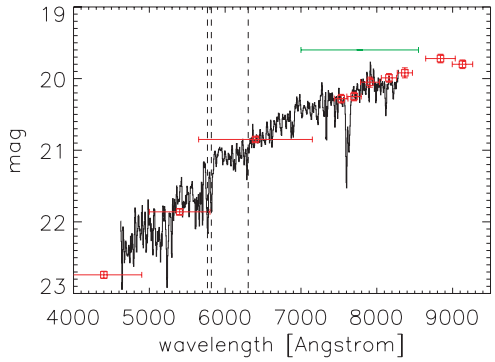

Figure 2. Spectral energy distribution of the lensing galaxy: The NTT spectrum (black) and the total magnitudes (red points). Dashed vertical lines show the positions of the strongest spectral features (Ca, H and K bands, and G band). The horizontal green bar gives the approximate common wavelength range covered by the F775 and F814 filters.

(A color version of this figure is available in the online journal.)

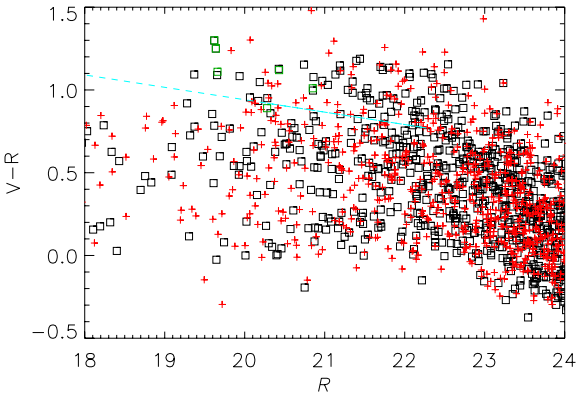

Figure 3. Color-magnitude diagram of the galaxies within 1 Mpc of the gravitational lens (black boxes), compared with the sources from the whole OACDF survey (red cross). Galaxies at redshift $z = 0.46 \pm 0.01$ in the same spatial region are shown as green boxes. The overplotted line is the fitted red sequence in galaxy clusters at $z \sim 0.45$ observed by De Lucia et al. (2007).

(A color version of this figure is available in the online journal.)

of 2.3 Å/pixel. The spectral resolution is $\simeq$10 Å; the signal to noise (S/N) about 8. Details of the data reduction are given in Alcalá et al. (2004). The NTT spectrum is shown in Figure 2, with the OACDF broad- and narrow-band imaging photometry overplotted. Some features typical of an early-type galaxy are apparent (the 4000 Å break, the H and K Ca II absorption bands), thus confirming the S0 classification and providing the redshift estimate $z_l = 0.466 \pm 0.005$. No clear feature from the lensed source was observed because of the low S/N: the average surface brightness of the arc, $\mu_{814} \simeq 22.0\,\mathrm{mag\,arcsec^{-2}}$, is too faint to provide identifiable spectral features other than strong emission lines.

In order to measure the redshift of the gravitational arc, on 2008 May 9 we obtained a spectrum of OAC–GL J1223–1239 with an exposure time of 3 × 1200 s using the 300 lines/mm grating of Keck/LRIS and a slit 1″ wide centered on the arc and aligned along the disk axis.

The blue side of the instrument used a 300 lines/mm grating blazed at 5000 Å; the red side used a 600 lines/mm grating blazed at 7500 Å. A dichroic at 6800 Å allows a single exposure to sample the wavelength range 3500–9400 Å. The spectral resolution in the blue and red parts of the spectrum was 8.5 Å and 3.8 Å, respectively. Despite the good seeing conditions ($\sim$ 0.″7), the spectrum does not allow us to disentangle the arc from the lens. Also, no clear feature from the arc is apparent, owing possibly to the abundance of atmospheric emission toward the red end of the spectrum. The superior spectral resolution of Keck/LRIS gives a more precise redshift for the lensing galaxy of $z_l = 0.4656 \pm 0.0004$.

The rest-frame absolute magnitude of the lens galaxy, derived from the broad-band photometry (see Table 1) assuming a negligible extinction[13] is $M_B = -20.7 \pm 0.1$. Thus OAC–GL J1223–1239 is an intermediate luminosity galaxy (in the sense of the Schechter luminosity function's parameter L_*) since, at $z \sim 0.45$, the absolute magnitude of L_* galaxies is $M_B^* = -20.78 \pm 0.17$ (Bell et al. 2004).

The color of OAC–GL J1223–1239, $(V - I) = 1.81$, is close to that of early-type galaxies in clusters at the same redshift. For instance, in the sample of objects at $z \sim 0.47$ within the ESO Distant Cluster Survey (De Lucia et al. 2007), galaxies at $I \sim 20$ on the red sequence have $(V - I) \simeq 1.65$.

[13] $E(B - V)$ is below 0.03 all over the OACDF; see Burstein & Heiles (1982).

Table 3
Parameters of the Best Gravitational Lensing Model

χ^2/n.d.f.	1.28
Axis ratio	0.55 ± 0.06
P.A. [deg]	-26 ± 5
External shear γ	0.080 ± 0.026
θ_γ (deg)	-72 ± 20
Magnification	$\sim$12
σ_L (z_s=0.9) (km s^{-1})	204 ± 3
σ_L (z_s=1.6) (km s^{-1})	170 ± 3

3. THE LENSING MODEL AND THE TOTAL MASS WITHIN R_E

The mass distribution of the lens component of OAC–GL J1223–1239, which must reproduce the morphology of the arc and of the counter image, was modeled by a singular isothermal ellipse (SIE) plus a contribution from an external shear γ to take into account the effects of the galaxies close to the line of sight. The $\sim r^{-2}$ total mass density profile of the our model is motivated by several statistical studies of lens samples. For instance, Koopmans et al. (2006) find that the slope of the total mass profile is isothermal at any redshift in the sample of SLACS lensing galaxies. The parameters of the model were fit by means of the `lenstool` software[14] (Kneib 1993), based upon a Bayesian Monte-Carlo–Markov chain optimization method (see Jullo et al. 2007 for details). The critical lines of the best SIE model are drawn in Figure 1, and the parameters listed in Table 3.

The best lensing model includes some external shear, possibly due to a local galaxy overdensity. The presence of a group of galaxies at z_l is supported by both photometric and spectroscopic data. A color-magnitude diagram of the galaxies within 4 arcmin (i.e., a projected radius of $\sim$ 1 Mpc) from the lensing galaxy, compared with the distribution of galaxies from the whole OACDF survey (see Figure 3), shows a dozen $L > L_*$ galaxies located along a red sequence close to the one observed at $z \sim 0.45$ by De Lucia et al. (2007). Six galaxies have spectroscopic redshifts in the range $z = 0.46 \pm 0.01$, including the OAC–GL J1223–1239 and a system of two bright ellipticals (CSL1, $z =$

[14] Publicly available at www.oamp.fr/cosmology/lenstool/.

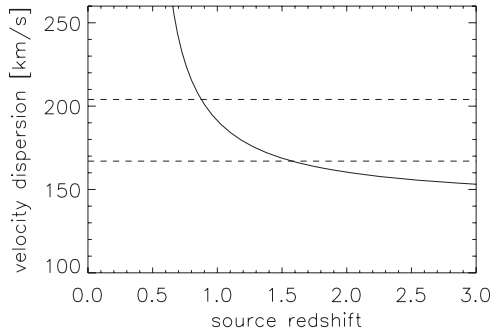

Figure 4. Velocity dispersion of the best SIE lens model as a function of the source redshift. Dashed lines correspond to the two FJ estimates (see the text for details).

0.463; M. Paolillo et al. 2008, in preparation) located at 53″ (220 kpc h^{-1}) from the lensing galaxy. Note that the spectroscopic survey of early-type galaxies in the OACDF was not spatially complete and did not cover the whole survey field. In particular, only $\sim 1/3$ of the region within 4.0 arcmin from the lens was covered by the masks.

The lensing model exhibits a small difference, $\Delta\theta = -13^\circ \pm 5^\circ$, in the orientation of the total mass model (i.e., dark and luminous matter) with respect to the light distribution (see Tables 2 and 3), which does not disappear by forcing a stronger external shear. This result is marginally consistent with Koopmans et al. (2006) who find, for lenses with velocity dispersion > 200 km s^{-1}, that the total mass is aligned with the light to within 10° (see also Kochanek 2002). Furthermore, the total mass distribution is more circularized ($q_{\rm SIE} = 0.55$) than the light ($q_{\rm star} = 0.35$).

This modeling points toward a geometry of the total mass different from that of the stellar mass, which in turn suggests the presence, within $R_{\rm E}$, of a DM component with a different spatial distribution than the light. By an iterative double-component approach with a spherical DM halo coupled to a flattened ($q_{\rm star} = 0.35$) stellar bulge, we find that, within $R_{\rm E}$, a DM mass $M^{\rm E}_{\rm dm}$ of the order of 25% of the total mass $M_{\rm T}(R_{\rm E})$ is sufficient to account for the ratio $q_{\rm SIE}/q_{\rm star}$ and to reproduce the observed image configuration. A larger DM fraction ($\sim 40\%$) is found for a nonspherical ($q \sim 0.8$) dark halo, in agreement with N-body simulations at this mass scale (Bullock et al. 2001), as well as weak lensing measurements (Hoekstra et al. 2004). It reduces to $\sim 35\%$ by forcing the halo to match the observed tilt.

In conclusion, this analysis constrains the dark mass fraction within the Einstein radius to 25%–35% of $M_{\rm T}(R_{\rm E})$.

Our model additionally provides the central velocity dispersion of the lensing galaxy as a function of the redshifts of the source and of the lens,

$$\sigma_{\rm L} = 144 \times \sqrt{\frac{D_{\rm s}(z_{\rm s})}{D_{\rm ls}(z_{\rm l}, z_{\rm s})}}\ {\rm km\,s^{-1}}, \qquad (1)$$

where $D_{\rm s}$ and $D_{\rm ls}$ are the angular diameter distances to the source and from the lens to the source respectively (see also Figure 4). The corresponding mass is

$$M_{\rm T}(R_{\rm E}) = 4.7 \times 10^{10}\, \frac{D_{\rm s}(z_{\rm s})}{D_{\rm ls}(z_{\rm l}, z_{\rm s})}\, M_\odot. \qquad (2)$$

For instance, with a source redshift ($z_{\rm s} = 1.6$) corresponding to the maximum strong lensing cross section of a lens at $z_{\rm l} = 0.466$, one obtains $\sigma_{\rm L} = 170$ km s^{-1} (see Table 3) and $M_{\rm T}(R_{\rm E}) = 7.0 \times 10^{10} M_\odot$.

We can compare the trend of $\sigma_{\rm L}$ with the value of the velocity dispersion $\sigma_{\rm FJ}$ derived from the Faber & Jackson relation (1976; hereafter FJ) applied to OAC–GL J1223–1239,

$$\frac{L}{L_*} = \left(\frac{\sigma_{\rm FJ}}{\sigma_*}\right)^{\gamma} \times 10^{\gamma_{\rm ev} z} \qquad (3)$$

corrected for galaxy passive evolution. Following Rusin et al. (2003), we adopt a B-band FJ slope $\gamma = 3.29$, $\sigma_* = 225$ km s^{-1}, and a passive evolution term $\gamma_{\rm ev} = -0.41$. The result $\sigma_{\rm FJ} = 204 \pm 28$ km s^{-1} is larger than the value obtained from the lens model with $z_{\rm s} = 1.6$, and requires a source redshift as low as $z_{\rm s} = 0.9$, implying $M_{\rm T}(R_{\rm E}) = 10.1 \times 10^{10} M_\odot$.

We note, however, that a large uncertainty still remains on the value of the critical parameter σ_*. For instance, Davis et al. (2003) argue in favor of a significantly lower value, $\sigma_* \sim 185 \pm 15$ km s^{-1}, by which we obtain $\sigma_{\rm FJ} = 167 \pm 23$ km s^{-1}, identical to the value of $\sigma_{\rm L}$ with $z_{\rm s} = 1.6$.

In summary, the FJ relation constrains $z_{\rm s}$ in the wide range 0.9–1.6, equivalent to a $\sim$30% variation of the total mass within the $R_{\rm E}$. This is three times larger than typical mass uncertainties at these radii (Kochanek et al. 2000) and does not independently allow to draw any firm conclusion on the DM content of the system.

However, besides the geometrical constraint discussed above $\left(M^{\rm E}_{\rm dm} \simeq 25\%{-}35\%\ M_{\rm T}(R_{\rm E})\right)$ and that given by the FJ relation ($144\ {\rm km\,s^{-1}} < \sigma_{\rm L} < 232\ {\rm km\,s^{-1}}$, including errors), we have still another card to play: we may estimate the stellar mass $M_*(R_{\rm E})$ within $R_{\rm E}$ from the spectrophotometric data.

The Keck/LRIS spectroscopic data allow us to measure the average velocity dispersion $\overline{\sigma}$ of the lensing galaxy over the region covered by the slit, which is $\sim 3 R_{\rm eff}$ wide and slightly off-center with respect to the galaxy nucleus (see Figure 1). The fit of the λ5892 absorption line profile gives $\overline{\sigma} = 150 \pm 11$ km s^{-1}. By modeling the galaxy as in N. R. Napolitano et al. (2008, in preparation), this figure returns an estimate of the central velocity dispersion in agreement with the lower value predicted by the FJ relation, i.e., $\sigma_{\rm FJ} = 170 \pm 15$ km s^{-1}. Mindful of the uncertainty intrinsic to this extrapolation, in the following analysis we will consider the whole range of values allowed by the FJ relation.

4. THE STELLAR MASS CONTENT WITHIN $R_{\rm E}$

The stellar mass-to-light ratio, M_*/L, has been derived by fitting the low-resolution spectrum (Figure 2) with the library of synthetic spectra by Bruzual & Charlot (2003). Since the choice of the initial mass function (IMF) is a critical point, we shall explore both Salpeter (1955) and Chabrier (2003) IMFs. A Salpeter IMF gives a global stellar mass-to-light ratio $M_*/L = 4.0\, M_\odot/L_\odot$, in the rest-frame B band, with an age of 8 Gyr and a subsolar metallicity ($Z = 0.004\, Z_\odot$). If M_*/L is uniform, from the total luminosity $L_{\rm B} = 2.7 \times 10^{10}\, L_\odot$ one obtains a total stellar mass $M_* = 1.1 \times 10^{11}\, M_\odot$.

In order to compute $M_*(R_{\rm E})$, the stellar mass within $R_{\rm E}$, it is prudent to disentangle the contributions of the two components, disk and bulge, which have different light profiles, isophotal geometry (see Table 2), and possibly mass-to-light ratios. Evolutionary synthesis models of template S0 galaxies of age ~ 8 Gyr predict a bulge mass-to-light ratio, $(M_*/L)_{\rm b}$, in excess of up to 1.5 times that of the disk, $(M_*/L)_{\rm d}$ (Buzzoni 2005). We use this upper limit to separate the contribution of the two components.

Table 4
Stellar Masses at the Einstein Radius

Salpeter IMF					
Model	M/L_b	M_b	M/L_b	M_d	$M_*(R_E)$
$M/L_b = 1.5 \times M/L_d$	4.4	5.4	2.9	0.3	5.7
$M/L_b = M/L_d$	4.0	4.8	4.0	0.4	5.2
Chabrier IMF					
Model	M/L_b	M_b	M/L_b	M_d	$M_*(R_E)$
$M/L_b = 1.5 \times M/L_d$	2.6	3.0	1.6	0.2	3.2
$M/L_b = M/L_d$	2.2	2.7	2.2	0.2	2.9

Note. Mass-to-light ratio are given in units of $M_\odot/L_\odot$ and stellar masses in units of $10^{10}\,M_\odot$.

By definition,

$$M_* = (M_*/L)_b \times L_{bulge} + (M_*/L)_d \times L_{disk}, \quad (4)$$

where $L_{bulge} = 1.9 \times 10^{10} L_\odot$ and $L_{disk} = 0.8 \times 10^{10} L_\odot$ from the measured bulge-to-disk ratio $B/D \sim 2.2$ (Table 2). Solving Equation (4) for a Salpter IMF, we obtain $(M_*/L)_d = 2.9\,M_\odot/L_\odot$ and $(M_*/L)_b = 1.5 \times M/L_d = 4.4\,M_\odot/L_\odot$. Thus, the bulge and disk masses within R_E are $M_b^E = 5.4 \times 10^{10} M_\odot$ and $M_d^E = 0.3 \times 10^{10} M_\odot$, respectively, with a total stellar mass $M_*(R_E) = 5.7 \times 10^{10}\,M_\odot$.

A simpler model with a single value of M_*/L gives a total mass (bulge+disk) within R_E of $5.2 \times 10^{10}\,M_\odot$ (Table 4).

Repeating the calculations with a Chabrier IMF, the stellar M_*/L ratio is ~ 1.8 smaller than with Salpeter ($M_*/L = 2.2\,M_\odot/L_\odot$ for the single population model, and $M/L_b = 2.6$, $M/L_d = 1.6\,M_\odot/L_\odot$ for the two population model), with the same age and metallicity assumed above. The stellar masses of bulge and disk are 1.8 times smaller, accordingly (Table 4).

5. COMPARING LENSING AND STELLAR MASSES

Since the quantity $M_T(R_E)$ remains parametrized with the source redshift (see Section 3), we now use the $M_*(R_E)$ values derived in the previous section to infer the range for z_s compatible with the other constraints. Figure 5 shows the trend for the projected DM fraction, $f_{dm}(R_E) = M_{dm}^E / M_T(R_E)$, as a function of the z_s, for both Salpeter and Chabrier IMFs, together with the constraints by the FJ relation and by the geometry of the system (green region). The redshift range allowed by all the constraints is $z_s = 1.2$–1.5 in the case of a single population model and $z_s = 1.1$–1.3, in the case of a composite disk+bulge population. The Chabrier IMF is highly inconsistent with the given limits.

In conclusion, considering a DM fraction (within R_E) in the range 25%–35%, the most likely solutions correspond to the redshift range $z_s = 1.3 \pm 0.2$ and favor the Salpeter IMF.

5.1. Interpreting the Favored Lens Model in the ΛCDM Framework

The total M/L within R_E varies from 4.7 ($z_s = 1.5$) to 6.1 ($z_s = 1.1$), with an average value of $M/L(R_E) = 5.4$–5.5 for $z_s = 1.3$. As shown in Section 4, considering just the baryons contribution, $M/L_* = 4.0$–4.4, allowing for the two-population model (Table 2); that is, the total M/L is a factor ~ 1.2–1.5 larger than the stellar M/L over the whole redshift range. These variations can be interpreted with the toy model from N+05 to infer the global properties of the virial DM content of the lensing system in the Λcold DM (ΛCDM) cosmology (see also Ferreras et al. 2005 for an application to a sample of lensing galaxies).

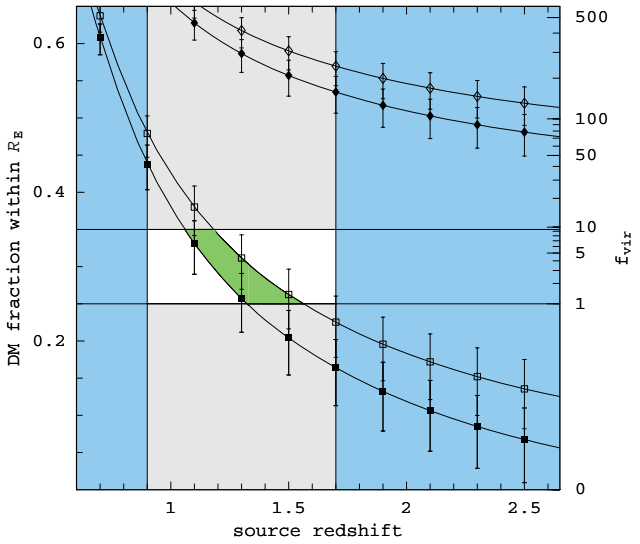

Figure 5. DM fraction at R_E versus the (unknown) redshift of the lensed source. On the right the corresponding (mean) f_{vir} values; see the text for details. Empty boxes are the DM fractions for the single bulge+disk population, full boxes for the two population models, assuming Salpeter IMF for the stellar M/L. Diamonds represent the same models for the Chabrier IMF. Gray denotes the regions excluded by the constraints on the f_{dm} from the lensing model geometry, cyan are the regions excluded by the Faber–Jackson relation. In green, the range of the parameter space allowed by all the constraints, accounting also for the uncertainty associated with the population models M/L.

(A color version of this figure is available in the online journal.)

We consider a multicomponent galaxy model with bulge stars distributed following a Hernquist (1990) profile with effective radius and total luminosity as from the first row of Table 2, disk stars following an exponential profile, with parameters as in the second row of Table 2, and a spherical DM halo with a Navarro, Frenk, & White (NFW; Navarro et al. 1997) density profile. As in N+05 and Bullock et al. (2001), we adopt the following concentration–mass relation for the DM halo,

$$c_{dm}(M_{dm}) \simeq \frac{1}{1+z} 17.1 \left(\frac{M_{dm}}{10^{11} M_\odot\, h^{-1}} \right)^{-0.125}, \quad (5)$$

where the concentration parameter is $c_{dm} \equiv r_{vir}/r_s$, with r_s the characteristic scale of the NFW profile, and M_{dm} is the total dark halo mass at the virial radius r_{vir}. The cumulative mass profile for a NFW dark halo is

$$M_{dm}(r) = M_{dm} \frac{A(r/r_s)}{A(c_{dm})}, \quad (6)$$

where

$$A(x) = \ln(1+x) - \frac{x}{1+x}. \quad (7)$$

We can now estimate the ratio $f_{vir} \equiv M_{dm}/M_*$, computing the NFW halo mass from Equations (5) and (6), and the stellar mass associated with the Hernquist (1990) model by using the photometric parameters of bulge and disk (see Table 2). Imposing that the modeled M/L is a factor ~ 1.2–1.5 larger than the stellar M/L within $R_E (\sim 1.15\,R_{eff})$,[15] we find $f_{vir} \sim 6 \pm 4$, for the whole galaxy. Here the main uncertainty

[15] This corresponds to a logarithmic M/L gradient, $\nabla\Upsilon \equiv \frac{R_{eff}\Delta\Upsilon}{\Upsilon_{in}\Delta R} \sim 0.2 - 0.3$ (see N+05) which is typical of local low-$\nabla\Upsilon$, i.e., low-DM systems.

comes from the choice of the stellar M/L, rather than from the halo concentration from the adopted $c_{dm}-M_{dm}$ (see e.g., Bullock et al. 2001) and the total $M/L(R_E)$ estimates. In Figure 5, the projected DM fraction is shown together with the corresponding values of f_{vir} as a function of the source redshift. If we consider the whole allowed range of z_s and the effect of the choice of the stellar M/L on the DM fractions, we see that the largest f_{vir} value is $\sim$20 for $z_s = 1.1$ (i.e., the lowest redshift allowed), while $f_{vir} < 20$ for $z > 1.1$, and $f_{vir} < 10$ for $z_s > 1.2$.

These values are consistent with the low global DM fraction regime at $z = 0$ discussed in N+05. These authors found a transition mass around $M_* = 1.6 \times 10^{11} M_\odot$ between more massive DM-dominated systems and low-mass, DM poorer systems. Incidentally, OAC–GL J1223–1239 is exactly located in this transition regime.

6. DISCUSSION AND CONCLUSIONS

OAC–GL J1223–1239, a $\sim L_*$ S0 galaxy at redshift $z = 0.466$, is among the least massive lenses at high redshift known to date. Although the source redshift is still not known, the observed phenomenology unambiguously supports the strong-lensing interpretation. The lensed source produces a bright arc (see Figure 1) with radius $0''.42$ ($\sim 1.15\ R_{eff}$ of the lens bulge). A candidate counter image is found at $0''.65$ from the lens center.

The total mass distribution, modeled by a SIE, is found to be rounder than the light at the Einstein radius, with a ratio $q_{SIE}/q_* = 1.84$, similar to the value found for galaxies with velocity dispersions lower than ~ 200 km s^{-1}.

We constrain the redshift of the source by coupling the value of the ratio $(M_{dm}/M_*)(R_E)$, obtained via the lens model, with the lens total mass within R_E, once the corresponding stellar mass $M_*(R_E)$ is evaluated by an assumption on the baryonic component and corresponding stellar M/L. We obtain $z_s \sim 1.3 \pm 0.2$ with a Salpeter IMF, the Chabrier IMF being ruled out. In this case, the velocity dispersion from the lens model (a SIE with an external shear) is $\sigma_L = 177^{+10}_{-6}$ km s^{-1} (with the given uncertainty derived from the allowed z_s range). This value is consistent with the limits imposed by the FJ relation.

OAC–GL J1223–1239 offers the possibility to investigate the mass distribution of the very inner region in an L_* galaxy at $z \sim 0.5$. Indeed, while there is growing evidence for a picture in which massive galaxies (i.e., above $\sim 10^{11.5} M_\odot$) are well described by an isothermal mass profile and show no structural evolution since $z \sim 1$ (see for instance, Treu 2007), we still lack a large sample of L_* galaxies at $z \gtrsim 0.5$ with a robust determination of the inner DM fraction in order to probe mass assembly and galaxy evolution at lower mass scales.

We find that OAC–GL J1223–1239 (assuming $z_s = 1.3$) has a projected DM fraction $\sim$ 30% within the Einstein radius. Lower values of the source redshift require a larger DM fraction in a nonspherical halo or a different IMF (e.g., Figure 5). By matching the measured mass-to-light ratio at the R_E with the one expected from a double-component model formed by a NFW spherical halo and a Hernquist (1990) spheroidal light distribution, we derive the total dark-to-luminous mass ratio $f_{vir} \equiv M_{dm}/M_* = 6 \pm 4$. This value is close to the one obtained for galaxies in the local Universe (Borriello et al. 2003; Romanowsky et al. 2003; N+05; Napolitano et al. 2009) located in the transition regime between massive DM-dominated galaxies and lower-mass, DM deficient systems.

A firmer estimate of the inner DM and stellar content in this L_* galaxy requires a further observational effort to determine the redshift of the lensed source. A possible strategy would involve, for instance, near-infrared spectroscopy aimed at detecting the H_α emission line.

The authors thank J. M. Alcalá and M. Pannella for allowing them to use the NTT spectrum of the lensing galaxy, C. Tortora for discussions on the derivation of the stellar mass from spectroscopic data, the Director of the Space Telescope Science Institute for granting Director's Discretionary Time, and the referee for constructive comments. G.C. and N.R.N. acknowledge funding from EC through the FP6-European Reintegration Grants MERG-CT-2005-029159 and MERG-CT-2005-014774, respectively. J.P.K. acknowledge support from CNRS. O.K. acknowledges INTAS grant Ref. No. 05-109-4793. NAG acknowledges support from grant HST-GO-10715.11-A.

REFERENCES

Alcalá, J. M., et al. 2004, A&A, 428, 339
Bell, E., et al. 2004, ApJ, 608, 752
Borriello, A., Salucci, P., & Danese, L. 2003, MNRAS, 341, 1109
Bruzual, & Charlot 2003, MNRAS, 344, 1000
Bullock, J. S., Kolatt, T. S., Sigad, Y., Somerville, R. S., Kravtsov, A. V., Klypin, A. A., Primack, J. R., & Dekel, A. 2001, MNRAS, 321, 559
Burstein, D., & Heiles, C. 1982, AJ, 87, 1165
Buzzoni, A. 2005, MNRAS, 361, 725
Capaccioli, M., Caon, N., & D'Onofrio, M. 1992, in ESO ESP/EIPC Workshop on Structure, Dynamics and Chemical Evolution of Early-type Galaxies (Elba), ed. J. Danziger, W. W. Zeilinger, & K. Kjar (ESO: Garching), 43
Capaccioli, M., Napolitano, N. R., & Arnaboldi, M. 2003, in Proc. for the Sakharov Conf. of Physics (Moskow), arXiv:astro-ph:0211323
Cappellari, M., et al. 2006, MNRAS, 366, 1126
Chabrier, G. 2003, PASP, 115, 763
Covone, G, Sereno, M., & de Ritis, R. 2005, MNRAS, 357, 773
Davis, A. N., Huterer, D., & Krauss, L. M. 2003, MNRAS, 344, 1029
De Lucia, G., et al. 2007, MNRAS, 374, 809
de Vaucouleurs, G. 1948, Ann. Astrophys., 11, 247
Douglas, N. G., et al. 2007, ApJ, 664, 257
Faber, S. M., & Jackson, R. E. 1976, ApJ, 204, 668
Faure, C., et al. 2008, ApJS, 176, 19
Ferreras, I., Saha, P., & Williams, L. L. R. 2005, ApJ, 623, L5
Hernquist, L. 1990, ApJ, 356, 359
Hoekstra, H., et al. 2004, ApJ, 606, 67
Jiang, G., & Kochanek, C. 2007, ApJ, 671, 1568
Jullo, E., et al. 2007, New J. Phys., in press, arXiv:0706.0048v1
Keeton, C. R., Kochanek, C. S., & Falco, E. E. 1998, ApJ, 509, 561
Kneib, J.-P. 1993, PhD thesis, Univ. of Toulouse
Kochanek, C. S. 2002, in Proc. Yale Cosmology Workshop, The Shapes of Galaxies and Their Dark Matter Halos, ed. P. Natarajan (Singapore: World Scientific), 62
Kochanek, C. S., et al. 2000, ApJ, 543, 131
Koekemoer, A. M., Fruchter, A. S., Hook, R., & Hack, W. 2002, *HST* Calibration Workshop, 337
Komatsu, E., et al. 2009, ApJS, in press, arXiv:0803.0547
Koopmans, L. V. E., et al. 2006, ApJ, 649, 599
Napolitano, N. R., et al. 2005, MNRAS, 357, 691 (N+05)
Napolitano, N. R., et al. 2009, MNRAS, in press (arXiv:0810.1291)
Navarro, J. F., Frenk, C. S., & White, S. D. M. 1997, ApJ, 490, 493
Nieto, J. L., & Bender, R. 1989, A&A, 215, 266
Peng, C. Y., et al. 2002, AJ, 124, 266
Romanowsky, A. J., et al. 2003, Science, 5640, 1696
Rusin, D., et al. 2003, ApJ, 587, 143
Salpeter, E. E. 1955, ApJ, 121, 161
Sazhin, M. V., Khovanskaya, O. S., Capaccioli, M., Longo, G., Paolillo, M., Covone, G., Grogin, N. A., & Schreier, E. J. 2007, MNRAS, 376, 1731
Treu, T., et al. 2005, ApJ, 633, 174
Treu, T., et al. 2006, ApJ, 640, 662
Treu, T. 2007, in Galaxy Evolution Across the Hubble Time, ed. F. Combes & J. Palous (Cambridge: Cambridge Univ. Press), 12